Mineral chemical evidence for extremely magnesian subalkaline melts associated with the Karoo large igneous province

Heinonen, Jussi S.

2010

acceptedVersion

Jussi S Heinonen (corresponding author)
(jussi.s.heinonen@helsinki.fi)
phone: +358 9 191 50805
Department of Geosciences and Geography
P.O. Box 64
FI-00014 University of Helsinki
Finland

Arto V Luttinen
(arto.luttinen@helsinki.fi)
phone: +358 9 191 28745
Finnish Museum of Natural History
P.O. Box 17
FI-00014 University of Helsinki
Finland

Mineral chemical evidence for extremely magnesian subalkaline melts from the Antarctic extension of the Karoo large igneous province

Abstract We present a comprehensive mineral chemical dataset (~400 analyses) on subalkaline meimechitic (Mg-number = 74–80) and ferropicritic (Mg-number = 67–69) dike samples from the Antarctic extension of the Karoo large igneous province (LIP) in Vestfjella, western Dronning Maud Land. Some of the meimechites, previously considered to be cumulates from ferropicritic magmas, are characterized by forsteritic olivine (with core composition up to Fo_{92}) that is in, or close to Fe-Mg equilibrium with the host rock. The olivines are subhedral to euhedral, contain Ti-rich (volcanic) spinel inclusions, have a high CaO content ($\geq$ 0.19 wt. %), and are thus unlikely to represent xenocrysts from mantle peridotite. Igneous amphibole is found in olivine-hosted, crystallized melt inclusions, indicating that the parental magmas had a H_2O content of 1–2 wt. %. The olivine data suggests generation of extremely MgO-rich (up to 25 wt. %) melts during the Karoo magmatism. Based on our petrogenetic modeling, such melts are likely to have originated from the partial melting of garnet peridotite at high pressures (5–6 GPa) and mantle potential temperatures (> 1600 °C) that are compatible with the involvement of a mantle plume in the generation of the Karoo LIP. A geochemical comparison of the Vestfjella meimechites with meimechites from the Siberian Traps LIP and the assumed komatiitic parental melts of the Horingbai picrites (Paraná-Etendeka LIP) reveals key similarities, suggesting that all these suites were generated from broadly similar sources and/or by similar melting processes in anomalously hot subcontinental mantle.

Key Words: Antarctica; ferropicrite; meimechite; petrogenesis; depleted mantle; Karoo; large igneous province; mantle plume

Introduction

The causes underlying the generation of continental flood basalts (CFBs) are still a matter of considerable debate. For example, opinions differ as to whether these huge manifestations of basic magmatism were associated with notable thermal anomalies in the mantle (e.g., mantle plumes; Richards et al. 1989; White and McKenzie 1989; Thompson and Gibson 2000) or if instead they formed by decompression melting related to plate tectonic processes (e.g., Anderson 2005; Elkins-Tanton 2005; Foulger 2007). One of the underlying factors in the debate is that CFBs are often characterized by fairly evolved compositions (MgO < 10 wt. %) and show strong lithospheric overprints in their geochemical signatures, thus hampering the identification of their parental magmas and sublithospheric mantle sources.

The CFBs of the Karoo large igneous province (LIP) were formed in an extensive rift system related to the break-up of the Gondwana supercontinent, with the highest volcanic activity occurring ~184–178 Ma ago (e.g., Duncan et al. 1997; Zhang et al. 2003; Jourdan et al. 2005, 2007b; Riley et al. 2005; Fig. 1a). Rocks with presumably undisturbed sublithospheric geochemical signatures are rare and typical of CFBs, and the origin of the Karoo basalts has also been debated (e.g., Burke and Dewey 1973; Cox 1978, 1992; Luttinen et al. 1998; Jourdan et al. 2005, 2007a; Riley et al. 2005; Curtis et al. 2008). Recently, ferropicrite dikes have been discovered in the Antarctic extension of the Karoo LIP, and there has been speculation on their sublithospheric geochemical affinities and potential plume sources (cf. Gibson et al. 2000; Gibson 2002; Riley et al. 2005; Heinonen and Luttinen 2008).
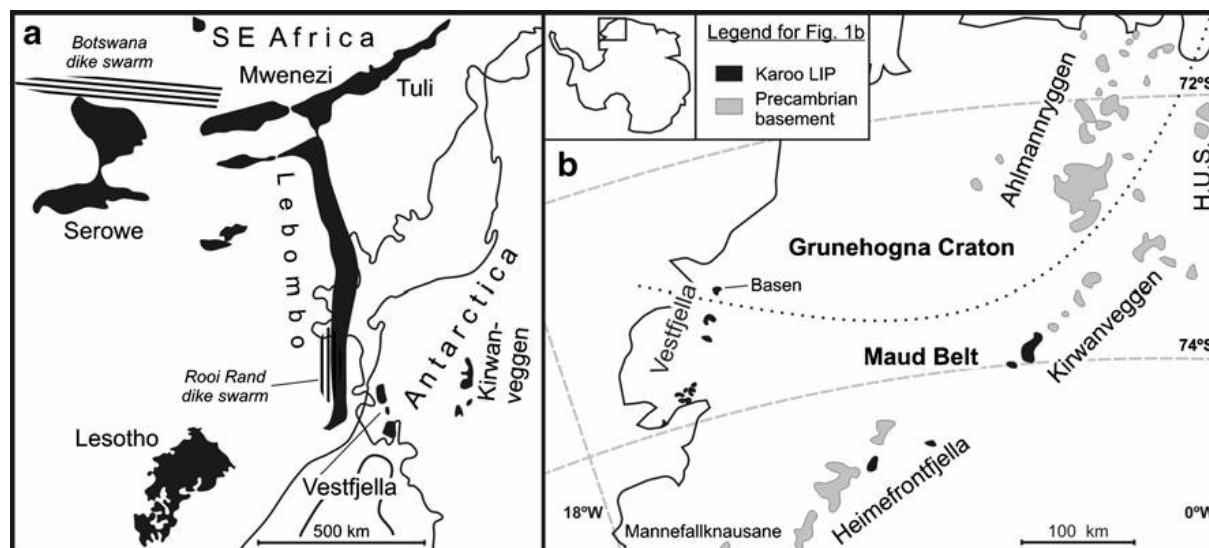

Fig. 1 Distribution of Jurassic continental flood basalts and related rocks in (a) reconstructed Karoo LIP and (b) western Dronning Maud Land. Gondwana reconstruction in (a) and lithospheric boundary in (b) are after Lawver et al. (1992) and Corner (1994), respectively. H.U.S. = H. U. Sverdrupfjella

In this paper, we present a comprehensive mineral chemical dataset on Karoo-related meimechites from Vestfjella, western Dronning Maud Land. These unusual rocks have been considered as cumulates derived from geochemically associated ferropicritic magmas (Heinonen and Luttinen 2008). We have estimated the compositions, including H_2O content,

and liquidus temperatures of the parental melts of the meimechites, by combining the mineral chemical data with previously published whole-rock geochemical data. The results show that at least some of the meimechites have been derived from extremely magnesian (up to 25 wt. % of MgO) parental melts that required a significant thermal anomaly (T_p > 1600 °C) in the sub-Gondwanan mantle.

Geological setting

The CFBs of western Dronning Maud Land comprise a volumetrically minor Antarctic extension of the Jurassic Karoo LIP (Fig. 1a) exposed at Vestfjella, Heimefrontfjella, and Kirwanveggen (Fig. 1b). Associated dikes are more widespread and also crosscut the Precambrian basement at Ahlmannryggen, Mannefallknausane, and H. U. Sverdrupfjella (Fig. 1b). The CFBs are mainly found overlaying Paleozoic sedimentary rocks (e.g., Juckes 1972), but at Vestfjella the basal contact of the lava pile is unexposed. The Phanerozoic rocks were deposited on a Precambrian basement complex, which is characterized by two main provinces: (1) the Grunehogna Province (Krynauw et al. 1991), which consists of an Archean basement (Barton et al. 1987) largely covered with Mesoproterozoic supracrustal rocks (Wolmarans and Kent 1982) and Neoproterozoic intrusions (Krynauw et al. 1991), and (2) the metamorphic Maud Belt (Groenewald et al. 1995), which accreted during a Grenvillian age orogenic event ~1100 Ma ago and was subsequently reworked by the Pan-African event ~500 Ma ago (Jacobs et al. 1998, 2003a, 2003b) (Fig. 1b).

Geochemically, the CFBs of western Dronning Maud Land consist mainly of tholeiites that show significant trace element heterogeneities; these heterogeneities have been thought to stem from the lithospheric contamination of ascending magmas and/or subduction-contamination of their mantle sources (e.g., Furnes et al. 1987; Harris et al. 1990; Luttinen et al. 1998; Luttinen and Furnes 2000). Some CFB-related rock types occur only as dikes: these include ferropicrites at Ahlmannryggen (Riley et al. 2005) and Vestfjella (Heinonen and Luttinen 2008) and 159 Ma lamproitic rocks at southern Vestfjella (Luttinen et al. 2002). It is likely that the absolute ages of the ferropicrites are between 190–163 Ma (Zhang et al. 2003; Riley et al. 2005; Heinonen and Luttinen 2008).

Ferropicrites of Vestfjella

The Vestfjella ferropicrites (MgO = 12–17 wt. %; FeO$_{tot}$ = 14–17 wt. %) crosscut the CFBs mainly as ~1–2 meter-wide dikes, striking approximately N-S or NE-SW. The dikes show geochemical division into two distinct types (Heinonen and Luttinen 2008): (1) The depleted type (two dikes) has La/Sm of 1.8–2.1, Sm/Yb of 3.9–4.2, and shows pronounced relative enrichment of V, but depletion of the most incompatible elements. (2) The enriched type (one dike) has La/Sm of 2.7–2.8, Sm/Yb of 4.7–5.0, and shows a general enrichment of incompatible trace elements resembling that of oceanic island basalts (OIBs). On the basis of primitive mantle-like contamination-sensitive trace element ratios and high initial ε_{Nd} (180 Ma) values (+3 to +8), the ferropicrites are not significantly contaminated with lithospheric material and, mainly due to their high FeO$_{tot}$ and TiO$_2$, are considered as partial melts from recycled pyroxenite sources (Heinonen and Luttinen 2008).

3

Meimechites of Vestfjella

The ferropicrites are associated with basaltic dikes (MgO < 12 wt. %) and meimechites (MgO > 18 wt. %) that, based on strong geochemical affinities, are thought to represent differentiates and cumulates from ferropicritic magmas, respectively (Heinonen and Luttinen 2008). Some of the meimechites represent central, cumulate parts of ferropicrite dikes, but most of them occur as very olivine-rich (26–49 vol. %) glacial boulders scattered over the top of the Basen nunatak, northern Vestfjella (Fig. 1b). Crosscutting relationships with sandstones and the lack of subaerial volcanic structures indicate that the boulders have a dike-origin. Geochemically, the meimechite boulder samples are relatively fresh (LOI = 0.7– 1.8 wt. %), subalkaline (SiO_2 = 44–53 wt. %; $Na_2O + K_2O$ = 1.3–1.8 wt. %), exhibit low Al_2O_3 (6–9 wt. %) and high FeO_{tot} (~ 13 wt. %) and MgO (19–28 wt. %) contents, and show trace element characteristics (e.g., La/Sm = 1.8–2.3, Sm/Yb = 3.2–3.5) that are very similar to those of the depleted type ferropicrites (Heinonen and Luttinen 2008; cf. Table 1). Due to their relatively high TiO_2 contents (1.3–1.7 wt. %), these rocks are classified as meimechites (TiO_2 > 1 wt. %) rather than komatiites (TiO_2 < 1 wt. %) (cf. Le Bas 2000).

Sample selection and analytical methods

Four samples from three meimechitic boulders and two samples from a depleted ferropicrite dike were selected for detailed mineral chemical analyses (Table 1). Sample AL/B1b-03 [Mg# = 74; Mg# = molar $Mg/(Mg+0.9Fe_{tot})$] was collected from a boulder of meimechite that forms a chilled margin contact with sandstone; the sample was taken 50 cm away from the margin. It is likely that meimechite boulder sample AL/B9-03 (Mg# = 79) represents the central parts of an eroded dike. Meimechite samples AL/B8a-03 (Mg# = 78) and AL/B8b-03 (Mg# = 80) were also collected from a boulder that shows a chilled margin contact with sandstone; the former is from close to the chilled margin whereas the latter was collected 70 cm away from the margin. Depleted ferropicrite samples AL/B14e-98 (Mg# = 67) and AL/B16-98 (Mg# = 69) are from the central portion of a ~2 m wide dike at Basen.

Mineral compositions were determined at the Geological Survey of Finland with a Cameca SX-100, using five wavelength-dispersive spectrometers. The apparatus was calibrated with a combination of natural and synthetic standards. The acceleration voltage, sample current, and beam diameter for the analyses were 20 kV, 20 nA, and 4 μm, respectively. The precision of the method was evaluated by performing repeated analyses on diopside and almandine standards: the coefficient of variation was below 1.6 % for all the major elements (> 5.0 wt. %) and below 3.3 % for all the minor elements (0.1–5.0 wt. %). Representative mineral analyses are presented in Tables 2–4; the complete dataset (~ 400 data points) is available in the Online Resource 1.

General petrography

All the analyzed samples are olivine-porphyritic (26–49 vol. % of phenocrysts; Fig. 2a) and samples AL/B16-98, AL/B14e-98, and AL/B1b-03 contain sparse clinopyroxene phenocrysts

4

(Table 1). Partially crystallized melt inclusions (up to 0.8 mm in diameter), consisting of varying amounts of Cr-spinel, amphibole, clinopyroxene, and chloritized mesostasis, are common in large olivine phenocrysts (Fig. 2b). The groundmass consists of clinopyroxene, plagioclase, Fe-Ti oxides, and sporadic brownish mica (Fig. 2a). All of the samples are relatively unaltered and contain fresh olivine. The detailed descriptions of the different mineral phases are given below.

Table 1 Descriptions and geochemical data for the samples selected for mineral chemical analysis (geochemical data published in Heinonen and Luttinen (2008))

Sample	AL/B1b-03	AL/B9-03	AL/B8a-03	AL/B8b-03	AL/B14e-98	AL/B16-98
rock type	meimechite	meimechite	meimechite	meimechite	ferropicrite	ferropicrite
description	boulder	boulder	boulder	boulder	~2 m wide dike	~2 m wide dike
	0.5 m from cm	dike center?	close to cm	0.7 m from cm	dike center	dike center
phenocrysts[§]	ol (27 vol. %) cpx (<1 vol. %)	ol (40 vol. %)	ol (45 vol. %)	ol (49 vol. %)	ol (26 vol. %) cpx (<1 vol. %)	ol (29 vol. %) cpx (<1 vol. %)
Major and minor elements (wt. %, normalized to 100% volatile free)						
SiO_2	46.57	45.53	45.00	44.07	46.75	45.38
TiO_2	1.61	1.44	1.57	1.31	2.49	2.47
Al_2O_3	8.31	7.01	6.84	5.77	8.58	8.76
FeO_{tot}	13.14	12.74	13.20	13.45	15.03	14.62
MnO	0.20	0.19	0.20	0.20	0.24	0.20
MgO	19.21	24.39	24.15	27.52	15.75	16.71
CaO	9.09	7.14	7.38	6.28	9.42	9.74
Na_2O	1.41	1.31	1.31	1.06	1.31	1.63
K_2O	0.34	0.15	0.23	0.23	0.21	0.28
P_2O_5	0.12	0.12	0.13	0.11	0.20	0.21
LOI (wt. %)*	1.55	1.04	0.68	1.07	3.76	1.07
Mg#**	74	79	78	80	67	69

[§] ol = olivine, cpx = clinopyroxene;* LOI = loss on ignition;** Mg# = Mg-number [atomic Mg/(Mg+Fe^{2+})*100; Fe^{2+}/Fe$_{tot}$=0.9]

Mineral chemistry

Olivine

The olivine is phenocrystic (≤ 6 mm in diameter), euhedral to subhedral, undeformed, and shows variable degrees of hydrothermal alteration to Fe-Mg layer silicates in general (Fig. 2a). Both ferropicrite samples (AL/B16-98 and AL/B14e-98) and meimechite samples AL/B1b-03 and AL/B9-03 also contain relatively small (< 3 mm in diameter) elongated olivine crystals that exhibit aspect ratios up to 10/1.

Representative olivine analyses are shown in Table 2. The olivine cores are Mg-rich with a range of Fo_{80-92} [$Fo_{88\pm3}$ (mean ± 1σ); n = 62] in meimechite samples AL/B1b-03 and AL/B9-03, Fo_{80-88} ($Fo_{84\pm1}$; n = 60) in meimechite samples AL/B8a-03 and AL/B8b-03, and Fo_{82-89} ($Fo_{85\pm2}$; n = 13) in the depleted ferropicrite dike. The olivine populations in meimechite samples AL/B1b-03 and AL/B9-03 are characterized by significantly more Mg-

rich compositions than those of meimechites AL/B8a-03 and AL/B8b-03, in which the compositions are more similar to olivines from the ferropicrite dike (Fig. 3a). The largest olivines are generally the most Mg-rich, whereas acicular and smaller crystals are relatively Fe-rich (Fig. 2a). Olivine exhibits normal zoning (ΔFo < 20 mol. %) that is generally observed only within ~0.2 mm of the outermost parts of the otherwise quite homogenous crystals.

The NiO content of the olivines is high (NiO = 0.2–0.5 wt. %) and shows positive correlation with the Fo content (cf. Fig. 3b). Furthermore, all olivines exhibit relatively high CaO content ($\geq$ 0.19 wt. %; cf. Fig. 3b).
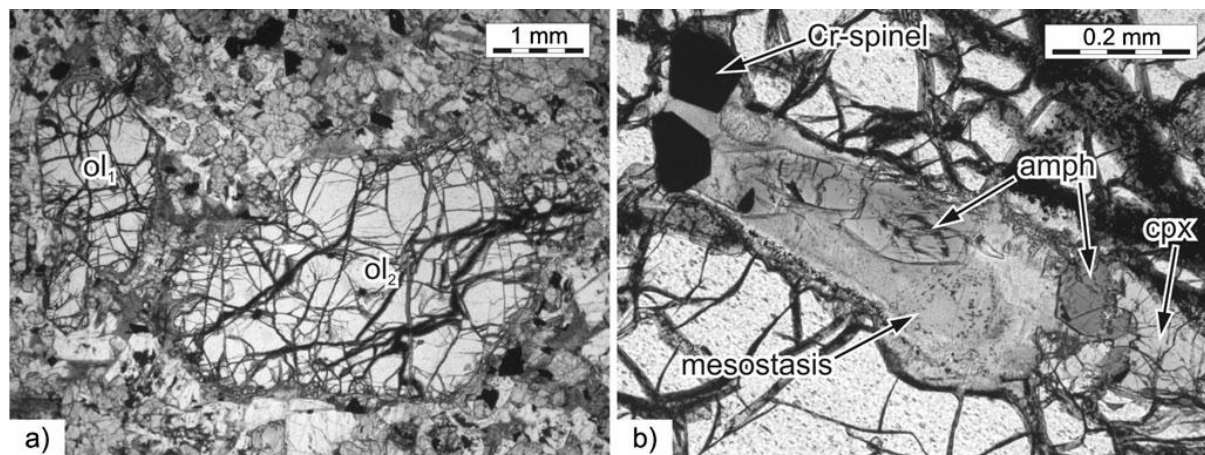

Fig. 2 Photomicrographs (plane-polarized light) of the Vestfjella meimechites: (a) olivine phenocrysts (ol_1=Fo_{85} and ol_2=Fo_{92}) in a groundmass consisting of clinopyroxene, plagioclase, and Fe-Ti oxides (sample AL/B1b-03); (b) olivine-hosted, partially crystallized
melt inclusion containing clinopyroxene (cpx), amphibole (amph), Crspinel, and chloritized mesostasis (sample AL/B1b-03)

Table 2 Olivine chemistry of the Vestfjella meimechites and depleted ferropicrite (Basen)

Sample	B1b/ r4/26	B1b/ 2/r3/46	B1b/ 2/r3/46r	B9/ r3/17	B9/ 12	B9/ 15	B8a/ r1/ol4	B8a/ ol27	B8b/ ol23	B14e/ r2/38
rock*	mmc(74)	mmc(74)	mmc(74)	mmc(79)	mmc(79)	mmc(79)	mmc(78)	mmc(78)	mmc(80)	fp(67)
position	core	core	rim	core	core	core	core	core	core	core
Oxides (wt. %)										
SiO_2	40.45	41.32	40.18	41.22	41.05	40.99	39.76	39.99	40.09	40.83
Al_2O_3	n.d.	0.08	0.05	0.05	0.07	0.08	0.04	0.04	n.d.	0.09
Cr_2O_3	0.09	0.16	0.07	0.10	0.12	0.14	n.d.	n.d.	n.d.	0.12
FeO	8.66	7.67	13.43	8.25	8.76	9.02	14.58	15.28	14.45	10.94
MnO	0.13	0.16	0.18	0.14	0.13	0.13	0.17	0.19	0.17	0.16
MgO	50.35	50.25	45.88	50.46	49.17	48.95	44.64	44.32	44.73	48.98
CaO	0.28	0.25	0.27	0.26	0.24	0.25	0.32	0.31	0.33	0.36
NiO	0.45	0.55	0.38	0.47	0.45	0.46	0.38	0.35	0.38	0.43
Total	100.41	100.44	100.44	100.95	99.99	100.02	99.89	100.48	100.15	101.91
End members (%)										
Fo	91.2	92.1	85.9	91.6	90.9	90.6	84.5	83.8	84.7	88.9
Fa	8.8	7.9	14.1	8.4	9.1	9.4	15.5	16.2	15.3	11.1

n.d. = not detected;* host rock: mmc = meimechite, fp = ferropicrite; Mg-number of the host rock shown in parentheses.
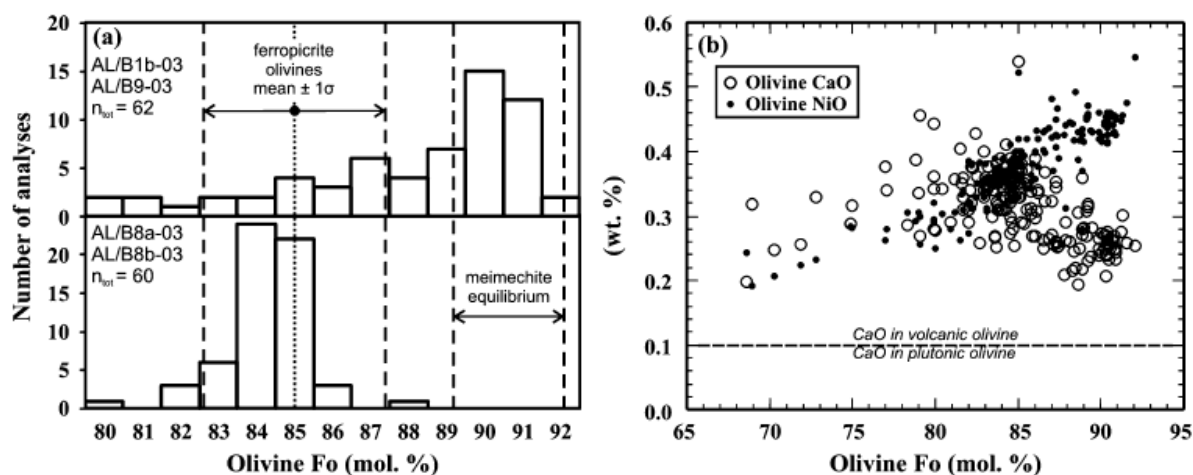
Fig. 3 Olivine chemistry of the Vestfjella meimechites and depleted ferropicrite (Basen) are shown in (a) histogram of olivine core analyses and in (b) CaO and NiO versus Fo diagram. The meimechite equilibrium field in (a) denotes the range of olivine compositions in Fe-Mg equilibrium (K_d=0.35; Fe^{2+}/Fe_{tot}=0.9) with the meimechite whole-rocks (Table 1; Heinonen and Luttinen 2008). The dashed line that separates volcanic and plutonic olivines on the basis of CaO in (b) is after Simkin and Smith (1970)

Cr-spinel

Cr-spinel is present within the crystallized, polymineralic melt inclusions (Fig. 2b) and as monomineralic inclusions in olivine phenocrysts. Cr-spinel microphenocrysts (< 0.05 mm in diameter) were also found within the relatively fine-grained groundmass of sample AL/B8a-03.

The compositions of the Cr-spinels show a relatively wide range of Cr_2O_3 (23–50 wt. %; Cr# = 57–77), Al_2O_3 (9–15 wt. %), FeO_{tot} (21–43 wt. %), and MgO (4–15; Mg# = 21–69) (Table 3; Online Resource 1). All the spinels have a notably high TiO_2 content ($\geq$ 1 wt. %) compared to spinels in peridotites. They plot within, or close to the fields of spinels in OIB and LIP in the discrimination diagram by Kamenetsky et al. (2001) (Fig. 4). MnO and ZnO contents are below detection limits.

Clinopyroxene

Clinopyroxene, whether occurring in the groundmass or as sparse phenocrysts, is generally euhedral to subhedral, unaltered, slightly reddish, and concentrically zoned.

The analyzed pyroxenes (Table 4; Online Resource 1) are Ti-rich (TiO_2 = 0.4–4.1 wt. %) augites (~84 %) and diopsides (~16 %). The Mg# [Mg# = $Mg/(Mg+Fe^{2+})$*100] of the clinopyroxenes varies between 96 and 57: the maximum Mg# (~80–90) of the groundmass clinopyroxenes is broadly similar in all the samples. The clinopyroxene phenocrysts exhibit somewhat higher Mg# (85–96 in cores), but are otherwise chemically very similar to groundmass clinopyroxenes (Fig. 5a, b). The concentrically zoned crystals show core-to-rim enrichment of TiO_2, Al_2O_3, and FeO_{tot}, and depletion of MgO (Fig. 5a, b).

Table 3 Cr-spinel chemistry of the Vestfjella meimechites and depleted ferropicrite (Basen)

Sample	B1b/ 2/r1/4	B1b/ 2/r2/25	B1b/ 2/r3/46	B1b/ 3/r5/27	B9/ r1/3	B9/ r2/9	B8a/ spl/28	B8a/ spl/33	B8b/ spl/46	B14e/ r4/33
rock*	mmc(74)	mmc(74)	mmc(74)	mmc(74)	mmc(79)	mmc(79)	mmc(78)	mmc(78)	mmc(80)	fp(67)
position	inclusion	inclusion	inclusion	inclusion	inclusion	inclusion	pc	inclusion	inclusion	inclusion
host olivine Fo	87.0	90.9	92.1	88.6	87.8	90.3	-	83.7	85.0	82.5
Oxides (wt. %)										
SiO_2	0.09	0.15	0.12	0.10	0.09	0.20	0.06	0.07	0.06	n.d.
TiO_2	1.39	1.06	1.66	1.20	1.49	1.27	3.55	3.00	2.10	3.14
Al_2O_3	9.50	10.10	14.10	10.85	10.28	11.18	11.43	12.53	12.05	10.77
Cr_2O_3	47.74	50.23	45.11	47.26	47.30	49.86	40.95	41.23	43.81	34.65
V_2O_3	0.16	0.10	0.12	0.17	0.16	0.15	0.34	0.40	0.27	0.30
Fe_2O_3**	11.06	9.14	10.69	8.46	9.71	8.91	12.09	12.13	10.90	20.00
FeO**	19.85	15.74	12.07	23.01	19.51	13.25	18.64	17.33	19.81	21.43
MgO	9.53	11.99	15.16	7.34	9.67	13.90	11.59	12.29	10.16	9.58
NiO	0.21	0.19	0.33	0.18	0.21	0.26	0.26	0.30	0.25	0.26
Total	99.52	98.70	99.35	98.57	98.40	98.99	98.90	99.27	99.41	100.14
FeO_{tot}	29.80	23.96	21.69	30.62	28.24	21.27	29.51	28.24	29.62	39.43
Fe^{2+}/Fe^{3+}	1.98	1.92	1.25	3.02	2.24	1.65	1.71	1.59	2.02	1.20
Mg#	46.2	57.6	69.1	36.2	46.9	65.2	52.5	55.9	47.8	44.3
Cr#	77.1	76.9	68.2	74.5	75.5	74.9	70.6	68.8	70.9	68.3

n.d. = not detected;* host rock: mmc = meimechite, fp = ferropicrite; Mg-number of the host rock shown in parentheses; pc = phenocryst. Fe^{2+}/Fe^{3+} (and FeO and Fe_2O_3) calculated on the basis of spinel stoichiometry; Mg# = $Mg/(Mg+Fe^{2+})*100$; Cr# = $Cr/(Cr+Al)*100$.
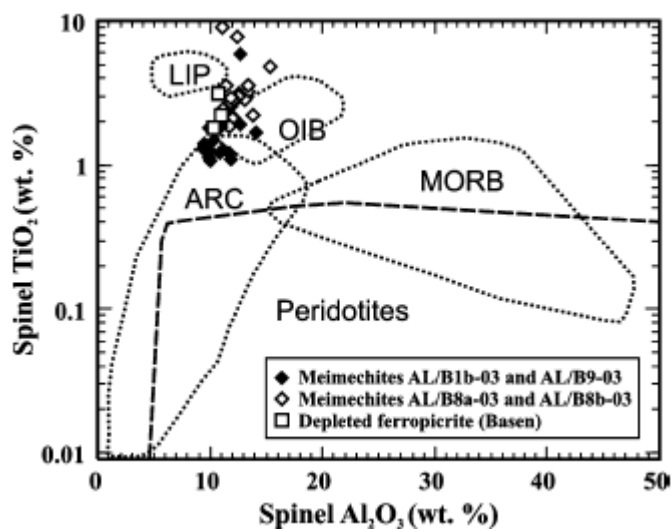

Fig. 4 Cr-spinel chemistry of the Vestfjella meimechites and depleted ferropicrite (Basen) are shown in the TiO_2 versus Al_2O_3 diagram. Spinel discrimination fields (LIP = large igneous provinces; OIB = oceanic island basalts; MORB = mid-ocean ridge basalts; ARC = island arcs; Peridotites = mantle peridotites) are after Kamenetsky et al. (2001)

Amphibole

Amphibole is present as small (< 0.3 mm in diameter), brownish, pleochroic, euhedral crystals within olivine-hosted melt inclusions in all the samples (Fig. 2b). The analyzed amphiboles can be classified as kaersutites (~63 %), hastingsites (~12 %), pargasites (~17

%), and tschermakites (~7 %) on the basis of 13eCNK normalization (cf. Schumacher 1997; Gualda and Vlach 2005) (Table 4). They exhibit compositions typical of igneous amphiboles (Fig. 6a; cf. Gilbert et al. 1982), show relatively large variations in TiO_2 (1–9 wt. %), Al_2O_3 (8–17 wt. %), FeO_{tot} (6–14 wt. %), and MgO (9–18 wt. %), and resemble amphiboles of Precambrian ferropicrites and komatiites (Fig. 6a, b).

Table 4 Clinopyroxene and amphibole chemistry of the Vestfjella meimechites and depleted ferropicrite (Basen)

Sample	B1b/ r4/24	B1b/ r6/32	B1b/ r6/35	B9/ r2/11	B8b/ r2/cpx2	B1b/ 2/r1/13	B1b/ 2/r4/58	B1b/ 3/r3/15	B9/ r1/5	B8a/ r1/amf2
rock*	mmc(74)	mmc(74)	mmc(74)	mmc(79)	mmc(80)	mmc(74)	mmc(74)	mmc(74)	mmc(79)	mmc(78)
position	gm	pc	pc(rim)	gm	gm	inclusion	inclusion	inclusion	inclusion	inclusion
(wt. %)										
SiO_2	51.18	52.70	50.21	49.18	51.62	40.95	39.46	41.42	41.98	38.73
TiO_2	0.67	0.51	1.20	1.58	0.86	3.87	6.22	4.99	4.23	5.45
Al_2O_3	2.82	2.05	3.51	5.63	2.57	14.36	15.00	13.24	15.28	16.52
Cr_2O_3	0.89	0.97	0.05	0.26	0.48	n.d.	0.12	0.46	n.d.	n.d.
FeO_{tot}	6.74	5.04	11.94	7.71	6.25	8.70	9.68	9.75	8.17	11.47
MnO	0.14	0.13	0.28	0.15	0.12	0.14	0.17	0.11	0.08	0.13
MgO	16.11	17.18	15.01	14.55	16.62	14.43	13.41	14.40	13.84	10.51
CaO	21.42	21.55	17.82	20.69	20.57	12.19	11.76	10.89	11.72	11.04
Na_2O	0.22	0.17	0.27	0.28	0.24	2.36	2.09	2.54	2.84	2.93
K_2O	-	-	-	-	-	0.15	0.13	0.22	0.09	0.09
F	-	-	-	-	-	0.19	0.11	0.42	0.18	0.16
Cl	-	-	-	-	-	n.d.	0.05	n.d.	n.d.	0.04
Total	100.19	100.30	100.29	100.03	99.33	97.34	98.20	98.44	98.41	97.07
Class	augite	augite	augite	augite	augite	pargasite	kaersutite	kaersutite	pargasite	pargasite
Mg#**	86.5	87.6	72.8	80.3	84.8	81.7	80.4	86.9	76.5	81.2
OH§ (cpfu)	-	-	-	-	-	~1.9	1.94	~1.8	~1.9	1.94

n.d. = not detected;* host rock: mmc = meimechite, fp = ferropicrite; Mg-number of the host rock shown in parentheses; pc = phenocryst; gm = groundmass. ** Mg# = $Mg/(Mg+Fe^{2+})*100$; Fe^{2+} calculated on the basis of 13eCNK normalization (cf. Schumacher 1997). § Assuming that atomic F + Cl + OH = 2 cpfu.
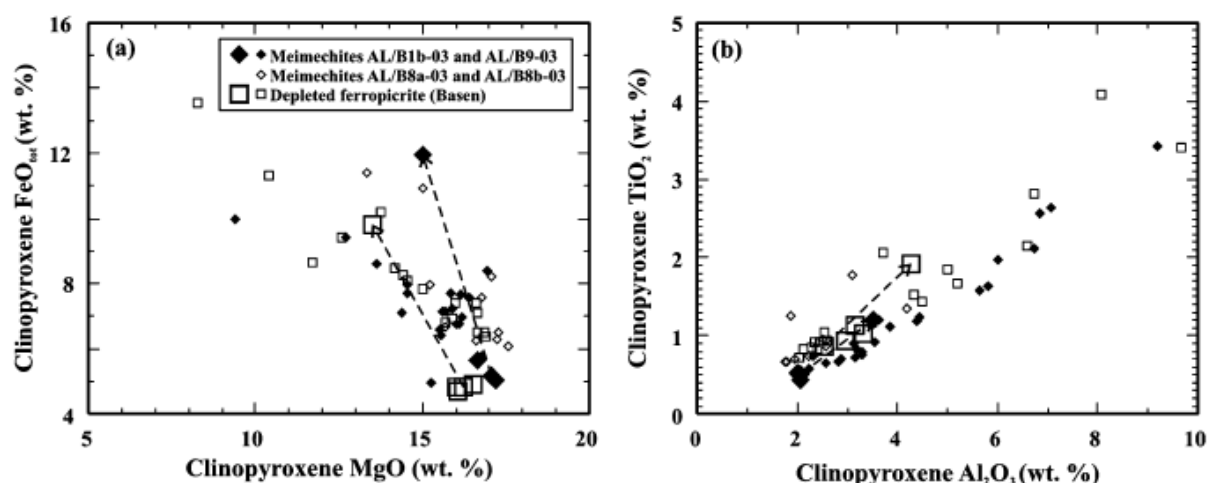

Fig. 5 Clinopyroxene chemistry of the Vestfjella meimechites and depleted ferropicrite (Basen) are shown in the (a) FeO_{tot} versus MgO and (b) TiO_2 versus Al_2O_3 diagrams. Symbol legend is given in (a). Large symbols indicate clinopyroxene phenocrysts and arrows indicate core-to-rim compositional progression
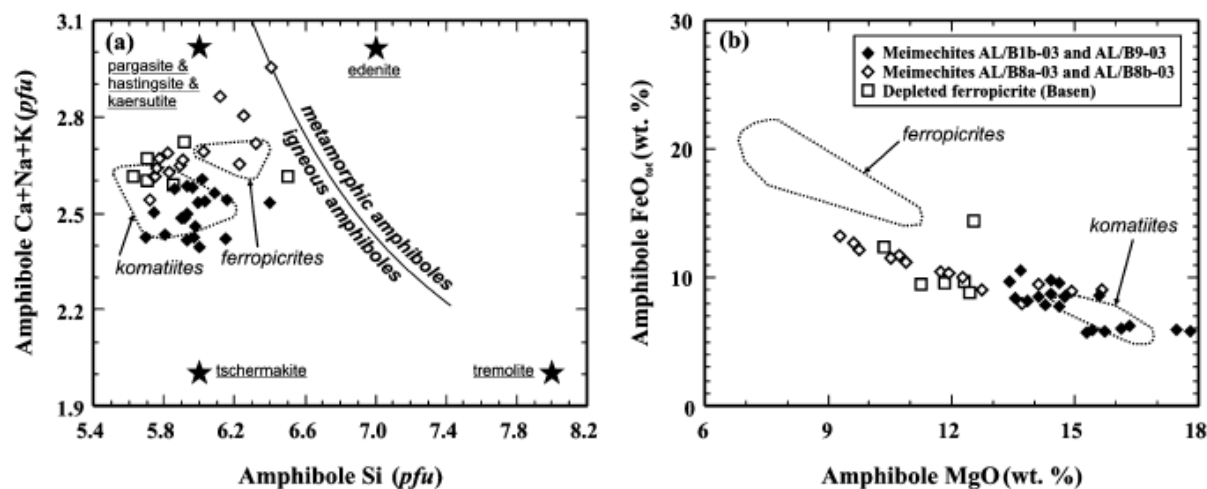
Fig. 6 Amphibole chemistry of the Vestfjella meimechites and depleted ferropicrite (Basen) are shown in the (a) Ca+Na+K versus Si (Leake 1971) and (b) FeOtot versus MgO diagrams. Amphiboles from Precambrian ferropicrites (Hanski 1992; Stone et al. 1997) and komatiites (Stone et al. 1997) are shown for comparison. Symbol legend is given in (b)

Other minerals

Plagioclase (An$_{63-40}$; Online Resource 1) generally forms subophitic to intergranular textures with adjacent groundmass clinopyroxenes. Fe-Ti oxides are also found in the groundmass as relatively small interstitial grains (< 0.5 mm in diameter) and have high Fe/Ti ratios characteristic of titanomagnetites (Online Resource 1). One small interstitial mica flake (~0.1 mm in diameter) analyzed from the meimechite sample AL/B1b-03 is a member of the biotite group (Online Resource 1).

Mineral-melt equilibria

Evidence for highly magnesian parental melts

The mineralogical data provides a means to address chemical equilibrium, i.e. to evaluate whether the whole-rock analyses correspond to melt compositions or are the result of magma mixing and/or crystal accumulation.

Meimechite samples AL/B8a-03 and AL/B8b-03 are characterized by olivines that are relatively Fe-rich (Fo$_{84-85}$), akin to olivine in the ferropicrite dike, and clearly out of Fe-Mg equilibrium with the whole-rock composition (Fig. 3a). These meimechite samples probably represent olivine cumulates from picritic or ferropicritic magmas (cf. Heinonen and Luttinen 2008) and, together with the ferropicrite samples, are excluded from the following discussion unless otherwise mentioned. Samples AL/B1b-03 and AL/B9-03 from two separate boulders, on the other hand, are characterized by forsteritic olivines (Fo$_{90-91}$) that are in, or close to being in Fe-Mg equilibrium with the host rock compositions (Fig. 3a). Furthermore, these olivines are euhedral to subhedral (Fig. 2a), homogenous, exhibit high CaO content typical of volcanic olivine (Fig. 3b; cf. Simkin and Smith 1970), and contain magmatic non-peridotitic spinel inclusions (Fig. 4) strongly supporting crystallization from primitive magmas; evidence for xenocrystic origin has not been observed. The origin of the relatively fewer,

10

somewhat more Fe-rich olivine grains is uncertain. Judging from their amphibole-bearing inclusions and primitive compositions, their origin is probably closely related to the meimechites. Some of them may represent Fe-enriched rims of large phenocrysts, or, alternatively, they could relate to settling of crystals in compositionally mildly-zoned meimechite dikes, or the mixing of meimechitic and ferropicritic magma pulses within the magma systems (cf. Larsen and Pedersen 2000). Nevertheless, their relative scarcity indicates that the geochemical effect of mixing and olivine accumulation on the whole-rock compositions was negligible.

Compositional data on the sparsely found clinopyroxene phenocrysts provide further evidence to support a relatively simple cooling history for the meimechites: The phenocrysts show uniform core compositions, normal zoning, general similarity to the groundmass clinopyroxenes (Fig. 5a, b), and are thought to represent rapid growth of clinopyroxene just before the cooling of the magma to near-solidus temperatures. Moreover, there is no geochemical evidence for the fractionation of clinopyroxene in ferropicrites or meimechites and the fractionation of Mg-rich olivine was mainly responsible for their magmatic differentiation (Heinonen and Luttinen 2008). Crucially, the geochemical compositions of the meimechites, as well as those of possible co-magmatic ferropicritic mixing end-members can thus be fractionation-corrected using conventional olivine-addition or -removal calculations.

The predominance of near-equilibrium olivine populations in samples AL/B1b-03 and AL/B9-03 indicates that they have crystallized from highly magnesian melts. The wide spread of the predominant, highly primitive olivine core compositions (Fo_{87-92}), however, indicates that some fractionation occurred during the cooling history (Fig. 3a). In order to discuss the petrogenesis of the meimechites in more detail, we calculated parental melt compositions for the primitive samples AL/B1b-03 and AL/B9-03 (that are characterized by forsteritic olivine) by adding olivine until Fe-Mg equilibrium with the most primitive phenocrysts ($Fo_{92.1}$ and $Fo_{91.6}$, respectively; Table 2) was achieved (cf. Albarède 1992; Larsen and Pedersen 2000; Putirka 2005, 2008a; Putirka et al. 2007). Based on the setting of the dikes within a thick continental lithosphere (> 200 km at present; cf. Morelli and Danesi 2004), as well as the sublithospheric affinities of the suite (Heinonen and Luttinen 2008), and the likelihood of rapid olivine nucleation after melt segregation, we used a $K_d(Fe–Mg)^{ol-liq}$ value of 0.35 that is compatible with pressures > 2.3 GPa (Putirka 2005). The $(Fe^{3+}/Fe_{tot})^{liq}$ ratio was calculated by using the experimentally constructed equation by Maurel and Maurel (1982; cf. Larsen and Pedersen 2000):

$$\log_{10}(Fe^{2+}/Fe^{3+})^{spl} = 0.764 * \log_{10}(Fe^{2+}/Fe^{3+})^{liq} - 0.343$$

The total range of resulting $(Fe^{3+}/Fe_{tot})^{liq}$ values was from 0.06 to 0.22. In our calculations, we used the value of 0.1 obtained from the most primitive spinels with the highest Cr#.

The results of the parental melt calculations are summarized in Table 5. In the case of sample AL/B9-03, only 2 wt. % of olivine needed to be added to reach the equilibrium composition, so that the whole-rock composition in Table 1 in fact provides a reasonably good estimate of the parental melt. Sample AL/B1b-03 is less magnesian and up to 21 wt. % of olivine had to be added to reach equilibrium with the most primitive olivine phenocrysts in this sample; the fractionation-corrected parental melt composition closely resembles that of

sample AL/B9-03 (Table 5). Given that at least some of the relatively Fe-rich olivine crystals (Fo_{80-86}) may represent incorporated material, most probably derived from ferropicritic magma, the whole-rock compositions and, thus, the starting melt compositions may be biased. Judging from the proportion of relatively Fe-rich olivine grains, the possible amount of excess olivine is likely to be less than 25% of the olivine phenocrysts, i.e. <10 wt. % in AL/B1b-03 and <15 wt. % in Al/B9-03 (cf. Table 1). Bearing in mind the relatively narrow range of olivine compositions and that any magmas that were possibly involved with meimechite petrogenesis probably represent relatively similar, olivine-controlled compositions, the mixing curves are nearly linear. Accordingly, the uncertainties related to the starting melt compositions preclude a reliable estimation of the amount of olivine addition, whereas the calculated parental melt compositions are not susceptible to significant error. The calculated CIPW normative compositions of the meimechite parental melts indicate 41–43 vol. % of modal olivine that closely corresponds to the amount of olivine in sample AL/B9-03 (40 vol.%); this suggests that our model parameters are feasible.

Table 5 Estimated parental melt compositions for the Vestfjella meimechites, Siberian meimechites, and Horingbai picrites, and whole-rock data for a representative Gorgona picrite

suite	Vestfjella	Vestfjella	Siberia	Horingbai	Gorgona
sample*	m1	m2	S2	calculated	GOR514
SiO_2 (wt. %)	45.5	45.5	40.2	46.9	46.5
TiO_2	1.3	1.4	3.6	0.7	0.3
Al_2O_3	6.6	6.9	4.5	9.1	10.4
FeO_{tot}	12.3	12.7	13.3	10.9	10.2
MnO	0.2	0.2	0.2	0.2	0.2
MgO	25.3	24.8	26.9	24.3	23.0
CaO	7.3	7.0	8.2	6.6	8.6
Na_2O	1.1	1.3	1.3	1.1	0.6
K_2O	0.3	0.1	1.5	0.1	0.2
P_2O_5	0.1	0.1	0.6	0.1	0.0
H_2O	1–2	1–2	0.5–3	0?	0?
Mg#	80.3	79.5	80.0	79.8	81.7

* m1 and m2 calculated on the basis of olivine-liquid equilibria using samples AL/B1b-03 and AL/B9-03 (Table 1; Heinonen and Luttinen 2008) as starting compositions, respectively (see text). S2 from Sobolev et al. (1991; cf. Elkins-Tanton et al. 2007; water contents from Elkins-Tanton et al. 2007), Horingbai melt composition from Thompson and Gibson (2000), and GOR514 from Révillon et al. (2000). Major and minor elements normalized to 100% volatile free and Mg# = $Mg/(Mg+Fe^{2+})*100$; Fe^{2+}/Fe_{tot}=0.9.

We also used the PRIMELT2 program by Herzberg and Asimow (2008) to place constraints on the primary melt compositions of the meimechites. In summary, PRIMELT2 can be used for calculating primary melt compositions of given rock samples and for evaluating whether or not such melts can be linked to a known mantle source. Assuming a mantle source similar to KLB-1 peridotite (see below), the primary melts calculated by PRIMELT2 for meimechite samples AL/B9-03 and AL/B1b-03 at 5 GPa pressure and Fe^{2+}/Fe_{tot} = 0.9 have MgO of 23–26 wt.% and closely resemble the fractionation-corrected compositions listed in Table 5 (Online Resource 2). More MgO-rich precursory melts are

very unlikely and, accordingly, we consider the fractionation-corrected compositions of samples AL/B1b-03 and AL/B9-03 to represent primary melt compositions.

Igneous amphibole: evidence for hydrous parental melts

The presence of Ti-, Al-, and Na-rich and Si-, Cl-, and F-poor amphiboles as euhedral crystals within olivine-hosted melt inclusions (Fig. 2b) suggests crystallization from high-T hydrous magmas (Fig. 6a; cf. Gilbert et al. 1982). Assuming that the depleted ferropicrites and meimechites are not significantly contaminated (Heinonen and Luttinen 2008), the water required to stabilize amphibole has been inherited from the mantle and not, for example, through interaction with water-rich crustal rocks. The absence of groundmass amphiboles in the samples may indicate that the magmas underwent extensive degassing at crustal levels or that the pressures were not high enough to stabilize amphibole during the late stages of crystallization. The rarity of other hydrous phases in the groundmass of the samples favors the former alternative.

Experimental studies indicate generation of calcic hydroxyl amphiboles in mafic magmas at temperatures of $\leq$ 1100 °C and H_2O^{liq} contents of $\geq$ 3.0–4.0 wt. % (Boyd 1959; Semet and Ernst 1981; Sisson and Grove 1993). Assuming a minimum H_2O content of 3 wt. % for the amphibole supersaturated melt and correcting for the crystallization of earlier phases, it is possible to estimate the H_2O content of the parental melts (cf. Stone et al. 1997). The amount of Cr-spinel and clinopyroxene in the melt inclusions and the $\leq$ 0.2 mm thick Fe-enriched zone in the host olivine roughly correspond to 50–60 % crystallization prior to amphibole supersaturation, suggesting ~1–2 wt. % H_2O in the parental melts. This result is compatible with the estimates presented by Stone et al. (1997) on the initial melts of amphibole-bearing Precambrian komatiites and ferropicrites (Fig. 6a, b). The role of water in the petrogenesis of ultramafic magmas is likely to promote partial melting, decrease both the density and viscosity of the parental melts, and thus favor their rapid ascent through lithosphere without significant interaction with country rocks (cf. Arndt et al. 1998).

Olivine-liquid equilibration and mantle potential temperatures

Our estimates of the meimechite parental melt compositions (Table 5) combined with the mineral chemical data on the most primitive olivine phenocrysts ($Fo_{92.1}$ and $Fo_{91.6}$; Table 2) can be used as a tool for calculating olivine-liquid equilibration temperatures (T^{ol-liq}) for the melts and potential temperatures (T_p; McKenzie and Bickle 1988) for the mantle beneath the Karoo LIP at the time of its emplacement (cf. Beattie 1993; Putirka 2005; 2008a; Putirka et al. 2007).

We have used the equations of Putirka et al. (2007) and Ford et al. (1983) for the olivine-liquid thermometry. As the melts probably originated beneath thick continental lithosphere (cf. Morelli and Danesi 2004), we considered the olivine-liquid equilibrium to be within a pressure range of 3–6 GPa; the lower value corresponds to the estimated equilibration pressure conditions of Hawaiian magmas (Putirka et al. 2007), whereas the latter corresponds to equilibration at a depth of ~200 km and is also compatible with pressure estimates derived from peridotite melting experiments (Fig. 7; see below). Conservative

pressure estimates ensure that T^{ol-liq} is not overestimated. Utilizing the equations of Putirka et al. (2007) (equation 4; cf. Putirka 2008b), the values for T^{ol-liq} range between 1599 °C and 1755 °C (Table 6). Such high temperatures are not surprising, given the exceptionally high MgO content of the rocks. In comparison, calculations made using the model by Ford et al. (1983) and the H_2O^{liq} correction by Falloon and Danyushevsky (2000), yield a significantly wider range of T^{ol-liq} between 1593 °C and 1791 °C: The temperatures are also invariably higher at pressures of 4–6 GPa, compared to those obtained with the model by Putirka et al. (2007) using the same parameters. Falloon et al. (2007) recently evaluated the accuracy of various olivine-liquid thermometers and, based on comparisons with experimental data, favored the model suggested by Ford et al. (1983). The treatment of Falloon et al. (2007), however, was based on experimental data at relatively low pressures (≤1.5 GPa) and the H_2O^{liq} correction method of Falloon and Danyushevsky (2000) was designed for relatively Mg-poor basaltic melts. We envisage that the generally lower temperatures obtained by using the equations by Putirka et al. (2007) are likely to be more suitable for highly magnesian melts generated at high pressures (cf. Putirka et al. 2007).

Olivine-liquid equilibration temperatures can be transformed into mantle potential temperatures using the equation $T_p = T^{ol-liq} + 667F - 13.3P$ (where F is the degree of melting and P is pressure; Putirka et al. 2007). It is widely accepted that the generation of mantle-derived magmas involves polybaric melting and, in general, the degree of melting is likely to be inversely related to pressure (cf. Putirka et al. 2007). Given that the incompatible element characteristics of magmas generated by polybaric melting may be dominated by relatively low-degree melt fractions, and that the major elements are more likely to reflect relatively high-degree melt fractions (Eggins 1992), we have sought feasible minimum and maximum F-values using rare earth element (REE) modeling and experimental major element data, respectively. Our REE-model aims to reproduce the meimechite REE-characteristics by partially melting the depleted MORB mantle (Online Resource 3): The batch melting model is compatible with F ≈ 3 % for the meimechite parental melts. In order to constrain the maximum F-value, we compared the parental melts in Table 5 with experimental peridotite-derived melt compositions (Fig. 7; see detailed discussion below). The meimechite parental melts plot close to the melt fraction contour of F = 12 %. Based on the subalkaline nature of the meimechites and the likelihood of polybaric melting, we consider that the lower F-value represents the absolute minimum degree of melting and that the higher F-value is more likely to be an underestimate of the maximum degree of melting: a choice of relatively low F-values ensures that the calculated mantle potential temperatures listed in Table 6 are not overestimated. Calculations using F = 3–12 % and P = 3–6 GPa yielded T_p values of ~1639–1695°C (Table 6). Given that H_2O^{liq} is unlikely to be significantly higher than 2 wt. % (cf. Stone et al. 1997) and that the F-values at given pressures are conservative estimates, we suggest that the T_p beneath the Karoo LIP at the time of its emplacement was > 1600 °C. This corresponds to mantle that is at least ~200 °C hotter than beneath modern mid-ocean ridges (cf. McKenzie and Bickle 1988; Green et al. 2001; Putirka 2008a) and indicates the presence of a significant thermal anomaly in the sub-Gondwanan mantle. Such high sublithospheric mantle temperatures are difficult to explain solely by gradual heating beneath thick continental lid and/or radioactive element-enriched basal lithosphere (cf. Lenardic et al.

2005; Coltice et al. 2007; Lee et al. 2009) and, therefore, we consider a mantle plume (Morgan 1971) to be the most plausible explanation for the anomaly.
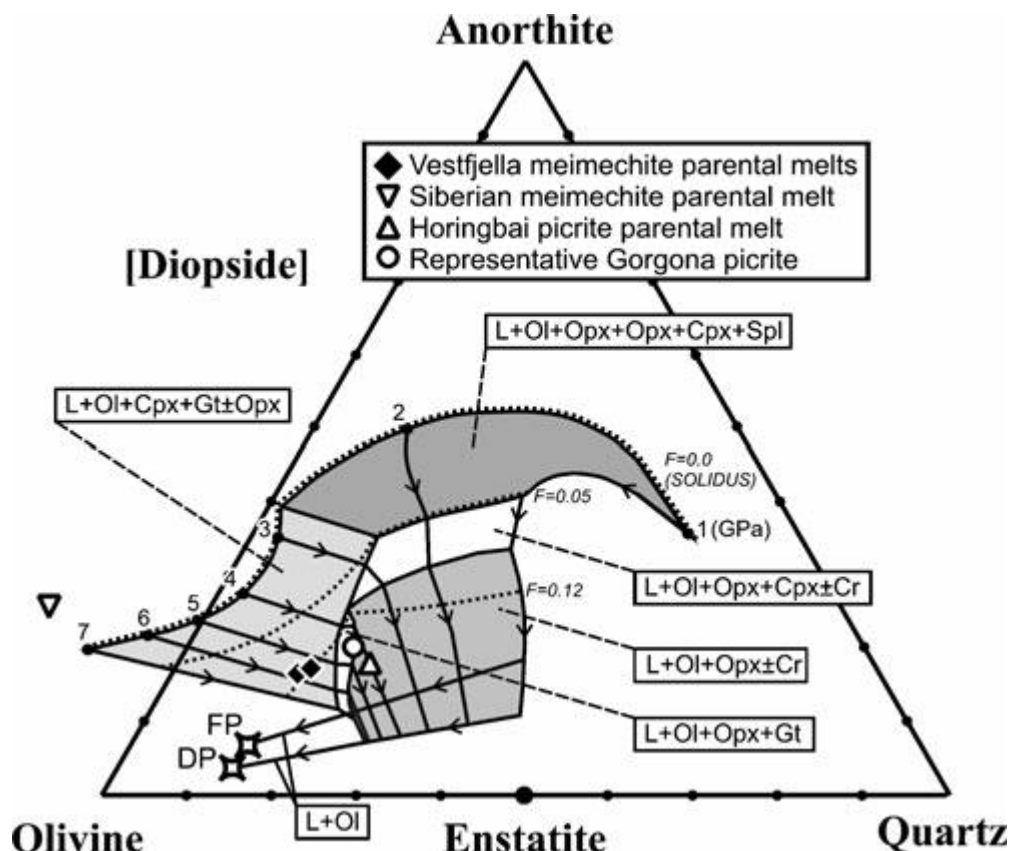

Fig. 7 Parental melt compositions for the Vestfjella and Siberia meimechites and Horingbai picrites, and whole-rock data for a representative Gorgona picrite (Table 5) are shown in projection from diopside and $Na_2O \cdot Si_3O_6$ and $K_2O \cdot Si_3O_6$ into the olivine-anorthite-silica plane (in mol %; after Herzberg and O'Hara 2002; Herzberg et al. 2007). Solid fields denote melt compositions in equilibrium with mantle peridotite at pressures of 1–7 GPa. Stippled lines indicate given melt fraction contours (F) and lines with arrows indicate estimates for cotectic equilibria at given pressures (cf. Herzberg and O'Hara 2002; Herzberg et al. 2007); arrows point up-temperature in the sense of advanced partial melting. Melts of depleted (DP) and fertile (FP) peridotite project along common cotectics, except when in equilibrium with olivine alone, or with olivine and orthopyroxene ± chromite (cf. Herzberg and O'Hara 2002)

Table 6 Olivine-liquid equilibration temperatures (°C) and mantle potential temperatures (°C; in parentheses) calculated for the Vestfjella meimechite parental melts (Table 5) at pressures of 3–6 GPa (degree of melting (F) = 0.12–0.03) and H_2O^{liq} contents of 1–2 wt. % following the method of Putirka et al. (2007) (see text)

	Parental melt of AL/B1b-03			
	3 GPa (F = 0.12)	4 GPa (F = 0.09)	5 GPa (F = 0.06)	6 GPa (F = 0.03)
H_2O=1 wt. %	1637 (1677)	1679 (1686)	1718 (1691)	1755 (1695)
H_2O=2 wt. %	1606 (1646)	1649 (1656)	1689 (1662)	1726 (1666)
	Parental melt of AL/B9-03			
	3 GPa (F = 0.12)	4 GPa (F = 0.09)	5 GPa (F = 0.06)	6 GPa (F = 0.03)
H_2O=1 wt. %	1629 (1669)	1671 (1678)	1711 (1684)	1748 (1688)
H_2O=2 wt. %	1599 (1639)	1642 (1649)	1682 (1655)	1719 (1659)

Implications on the nature of the mantle source

The parental melt compositions calculated based on olivine-melt equilibria (Table 5) provide a powerful tool for addressing the mantle sources of the meimechites. First and foremost, the extremely MgO-rich (~25 wt. %) character of the meimechite parental melt is a strong indication that it derives from a dominantly peridotitic mantle source: experiments on compositionally variable pyroxenitic starting materials have invariably yielded partial melts with MgO < 16 wt. % (cf. Kogiso et al. 2004).

There are two principal ways to generate ultramafic melts from mantle peridotite: high degrees of melting (increased olivine contribution) or melting at great depth (decreased olivine stability) (e.g., Herzberg and Zhang 1996). For example, judging from their high Sm/Yb and low Al_2O_3 values (cf. Heinonen and Luttinen 2008) and their setting within thick continental lithosphere (cf. Morelli and Danesi 2004), the Vestfjella meimechites originated at great depths. Herzberg and O'Hara (1998, 2002) combined an extensive set of experimental data in order to place constraints on liquid compositions that would exist in equilibrium with mantle peridotite at varying pressures. We have utilized their results to estimate melting conditions during production of the parental melts of the Vestfjella meimechites (Fig. 7). Although the model of Herzberg and O'Hara is not based on experimental data on H_2O-bearing systems, experimental peridotite partial melts with H_2O < 2.5 wt. % tend to be very similar to dry melts representing the same degree of melting (Hirose and Kawamoto 1995; cf. Herzberg and O'Hara 2002), thus enabling us to also use the model for H_2O-bearing Vestfjella meimechites.

In the diagram by Herzberg and O'Hara (2002), the parental melts of the Vestfjella meimechites plot within the field of peridotite supersolidus melts equilibrated with a garnet lherzolite residue at 5–6 GPa (Fig. 7), suggesting that the meimechites were generated by relatively low-degree melting of peridotite at high pressures. Importantly, as the meimechites show petrographical, mineralogical (Fig. 4–6), and geochemical (Fig. 8; Heinonen and Luttinen 2008) affinity to the depleted ferropicrites, the previously suggested pyroxenitic mantle sources for the latter may not be viable. In fact, the compositional affinities between meimechites and depleted ferropicrites, the presence of some exceptionally magnesian olivine phenocrysts (up to Fo_{89}; Table 2) in the depleted ferropicrites, and the success of PRIMELT2 modeling of depleted ferropicrite parental melt using KLB-1 peridotite (Online resource 2), collectively lend support to the supposition that the depleted ferropicrites derive from highly magnesian, meimechitic parental melts. Although our study suggests that the principal source of the Vestfjella meimechites and depleted ferropicrites was peridotitic, further isotopic and geochemical studies are needed in order to reliably evaluate the role of possible subordinate recycled sources in their petrogenesis (cf. Heinonen and Luttinen 2008).

Comparison with other highly magnesian Phanerozoic melts

Based on olivine-whole rock data, the Jurassic Vestfjella meimechites represent exceptionally magnesian subalkaline melts generated during the Phanerozoic eon. Although olivine-phyric primitive volcanic rocks are found in several Phanerozoic LIPs, the purported parental melts are typically considered as picrites with MgO ≤ 18 wt. %; evidence for more

magnesian parental melts has been recognized, e.g., in the Permian Siberian Traps LIP (e.g., Arndt et al. 1995; Kogarko and Ryabchikov 2000), Cretaceous Caribbean LIP (e.g., Herzberg et al. 2007), Cretaceous Paraná-Etendeka LIP (Thompson and Gibson 2000, Thompson et al. 2001), and the Tertiary North Atlantic LIP (Larsen and Pedersen 2000). To our knowledge, ultramafic parental melts that are as primitive as the Vestfjella meimechites (MgO 23–27 wt. %) have been associated only with the Gorgona "picrites" (komatiites according to the current classification scheme of Le Bas (2000)) of the Caribbean LIP, the Horingbai picrites of the Paraná-Etendeka LIP (based on Fo_{93} olivine macrocrysts), and the meimechites from the Maymecha-Kotuy region of the Siberian Traps LIP. We will focus our treatment of the Vestfjella meimechites on these extremely magnesian suites in order to identify possible petrogenetic similarities (and dissimilarities) between anomalous melting events associated with Phanerozoic LIP magmatism.
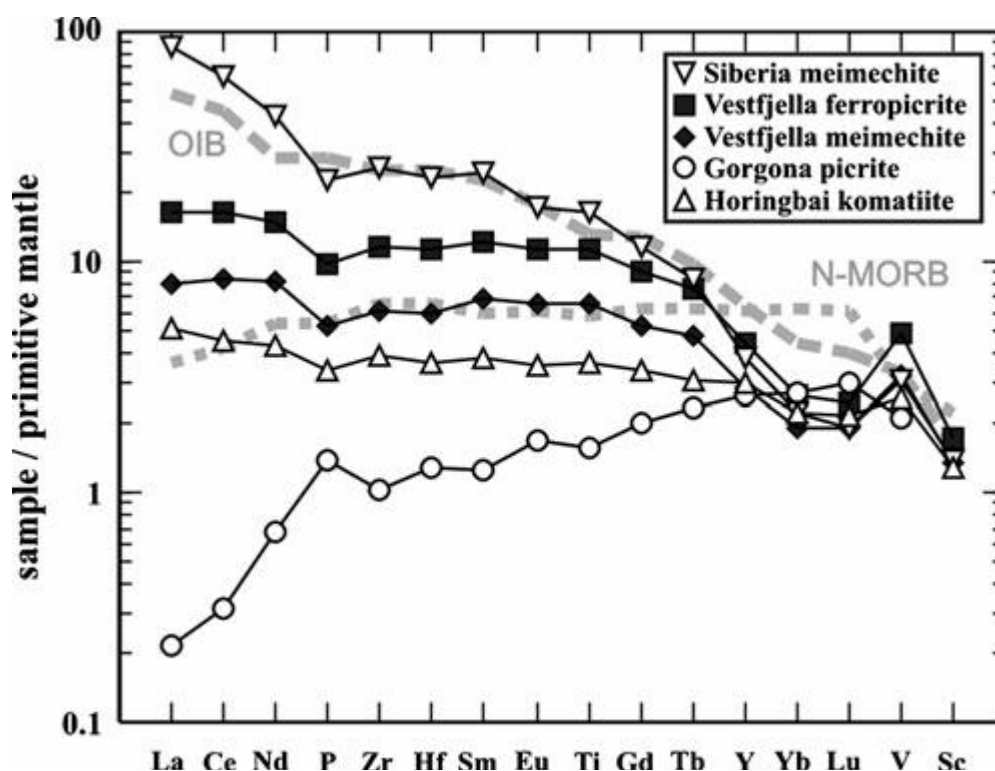
Fig. 8 Primitive mantle-normalized incompatible element patterns of representative meimechite (Al/B9-03) and depleted ferropicrite (AL/B16-98) samples from Vestfjella (Heinonen and Luttinen 2008). Average Siberian meimechite [n=13; compiled from the analyses of Arndt et al. (1995, 1998), Fedorenko and Czamanske (1997), Carlson et al. (2006), and Elkins-Tanton et al. (2007); cumulate samples ignored so that MgO_{avg}=27 wt. %], representative Gorgona picrite (sample GOR514 from Révillon et al. 2000; data for Sc not published), theoretical Horingbai komatiite (added ~35 wt. % of olivine into the whole-rock composition of sample 97SB53 so that MgO_{liq}=24 wt. %; Thompson et al. 2001) average N-MORB (Sun and McDonough 1989; V and Sc from Salters and Stracke 2004), and average OIB (Sun and McDonough 1989; V and Sc calculated after GEOROC: http://georoc.mpch-mainz.gwdg.de/georoc/) are shown for comparison. Normalizing values after Sun and McDonough (1989), except for V and Sc, after McDonough and Frey (1989)

The assumed parental melt compositions of the Gorgona picrites, the Vestfjella meimechites, the Siberian meimechites, and the Horingbai picrites are compared in Table 5 and Fig. 7–8. However, the major element composition of the parental melt for the Gorgona picrites and the trace element contents for the Horingbai parental melt have not been

constrained. Accordingly, we have used data from a representative Gorgona picrite sample, with MgO = 23 wt. %, corresponding to the estimated parental melt composition (cf. Herzberg et al. 2007), and fractionation-corrected trace element data from the least-contaminated Horingbai picrite (Thompson et al. 2001) to facilitate qualitative geochemical comparisons. We consider the parental melt compositions presented in Table 5 to provide fair approximations of primary melt compositions (cf. Thompson and Gibson 2000; Elkins-Tanton et al. 2007; Herzberg et al. 2007).

In general, the data for Gorgona, Horingbai, Vestfjella, and Siberia represent a collection of ultramafic melts with gradational geochemical characteristics (Table 5). The Gorgona picrite exhibits the lowest TiO_2 (0.3 wt. %) and FeO_{tot} (10.2 wt. %) and the highest Al_2O_3 (10.4 wt. %), compatible with the melting of highly depleted peridotite at relatively low pressure, possibly down to 2.5 GPa (Herzberg and O'Hara 2002; cf. Herzberg et al. 2007). In contrast, the Gorgona picrite plots at the boundary of the garnet harzburgite + liquid field of Fig. 7, close to the cotectic curve at 4–5 GPa. Given that the parental melts of the Gorgona picrites have been associated with dynamic fractional melting (Arndt et al. 1997; Herzberg and O'Hara 2002; Herzberg et al. 2007), however, comparison with cotectic equilibria in Fig. 7 is likely to yield incorrect pressure estimates (cf. Herzberg et al. 2007). In comparison, the purported Horingbai parental komatiite melt has somewhat higher TiO_2 (0.7 wt. %) and FeO_{tot} (10.9 wt. %) and lower Al_2O_3 (9.0 wt. %), in accordance with the generation of these magmas from depleted peridotite by relatively high-degree melting that began at relatively high pressures (up to 6 GPa; Thompson and Gibson 2000). Such a polybaric melting scenario is broadly compatible with plotting the Horingbai melt close to the 4 GPa cotectic within the harzburgite + liquid field of Fig. 7. The Siberian parental meimechite melt, on the other hand, shows notably high TiO_2 (3.6 wt. %), FeO_{tot} (13.3 wt. %) and low Al_2O_3 (4.5 wt. %), compatible with an extremely low degree of melting (<7 %, likely to be close to 1 %; Arndt et al. 1995; Carlson et al. 2006) at very high pressures (5.5–10 GPa; Arndt et al. 1998; Elkins-Tanton et al. 2007) (Table 5). Indeed, the Siberian parental melt plots close to the peridotite solidus at 6–7 GPa in Fig. 7.

The Vestfjella parental meimechite melts show compositions (TiO_2 = 1.3–1.4 wt. %, FeO_{tot} = 12–13 wt. %, and Al_2O_3 = 7 wt. %) that in many respects lie between the Horingbai and the Siberian parental melts (Fig. 7; Table 5); their position close to the lherzolite-harzburgite boundary in Fig. 7 is broadly compatible with our REE-based melting model (F ≈ 3%; Online Resource 3), suggesting a relatively low-degree (~12 %) of melting at 5–6 GPa. In polybaric melting scenarios, these melting parameters would be expected to represent average values (cf. Herzberg and O'Hara 2002).

Primitive mantle-normalized trace element patterns bring more detail to the geochemical comparison (Fig. 8). The Gorgona picrite exhibits a distinctive, relatively flat pattern with a strongly depleted light REE and other highly incompatible elements. The trace element pattern has been ascribed to the low-pressure melting of a highly depleted peridotite source generated by successive melting events (cf. Arndt et al. 1997; Herzberg and O'Hara 2002; Herzberg et al. 2007). The parental melts associated with Horingbai, Vestfjella, and Siberia show notably more enriched, but still variable incompatible element contents. The variable degree of incompatible element enrichment is broadly compatible with increasing degrees of partial melting in the order Siberia – Vestfjella – Horingbai (cf. Fig. 7). Despite

this difference, the patterns exhibit notably similar diagnostic features with characteristic positive V anomalies ($(V/Lu)_{PMN}$ = 1.2–1.7; Fig. 8) that distinguish them from the Gorgona picrites and typical MORB, OIB (Fig. 8), and LIP magmas (Heinonen and Luttinen 2008). Accordingly, the geochemical affinities shown in Fig. 7–8 imply broadly similar mantle sources and/or melting processes for the Horingbai komatiite and the two meimechite suites. We speculate that the distinctive compositional characteristics of these suites may be related to the onset of depleted mantle melting at exceptionally high temperatures ($\geq$ 1550 °C; Thompson and Gibson 2000; Elkins-Tanton et al. 2007; Table 6) and pressures ($\geq$ 5 GPa; Arndt et al. 1998; Thompson and Gibson 2000; Elkins-Tanton et al. 2007; Fig. 7). The depleted mantle sources may have differed from each other in terms of fluid characteristics: dry sources have been advocated for the Horingbai picrites (Thompson and Gibson 2000), whereas the meimechites of Siberia and Vestfjella have been associated with a source that was rich in volatiles (cf. Arndt et al. 1998; Ryabchikov et al. 2002; Carlson et al. 2006; Elkins-Tanton et al. 2007). In the case of Siberian meimechites, however, the source of volatiles has been attributed to a minor lithospheric component that has also been thought to account for a mild overprint on the incompatible element signatures and isotopic ratios (Horan et al. 1995; Elkins-Tanton et al. 2007). In contrast, Nd and Sr isotopic data on the ferropicritic correlatives of the Vestfjella meimechites do not reveal involvement of lithospheric material (Heinonen and Luttinen 2008), implying that the Vestfjella meimechites may be related to the melting of hot and volatile-bearing, deep asthenospheric mantle beneath a thick continental lithospheric lid.

Conclusions

On the basis of the mineralogical and geochemical data on the meimechites of Vestfjella from the Antarctic extension of the Karoo LIP, we present the following conclusions:

1. Some of the meimechites are characterized by Mg-rich olivine phenocrysts (Fo_{80-92} in cores) that are not xenocrysts and are either in, or close to Fe-Mg equilibrium with their respective host rocks, implying their crystallization from highly magnesian parental melts. In contrast, some other meimechites are cumulates derived from picritic parental melts.

2. All samples contain igneous amphibole within olivine-hosted inclusions, indicating substantial amounts of H_2O (~1–2 wt. %) in the parental melts.

3. The compositions (MgO $\approx$ 25 wt. %; FeO_{tot} $\approx$ 12–13 wt. %; Al_2O_3 $\approx$ 7 wt. %) of the calculated meimechite parental melts are compatible with derivation from a garnet-bearing peridotite at high pressures (5–6 GPa) and at very high mantle potential temperatures (> 1600 °C on the basis of olivine-liquid equilibria) that are most readily attributed to an upwelling plume in the deep sub-Gondwanan mantle.

4. The immobile incompatible element signatures of the Vestfjella meimechites show similarities (e.g., high V/Lu) to those of the meimechites from the Siberian Traps and the hypothetical parental melts of the Horingbai picrites (Paraná-Etendeka CFB), indicating that

these exceptionally MgO-rich magmas related to CFB events may have had broadly similar depleted mantle sources and/or may have been generated by similar melting processes beneath thick continental lithosphere.

Acknowledgements

References

Albarede F (1992) How deep do common basaltic magmas form and differentiate? J Geophys Res B 97:10, 997–11, 009

Anderson DL (2005) Large igneous provinces, delamination, and fertile mantle. Elements 1:271–275

Arndt N, Lehnert K, Vasil'ev Y (1995) Meimechites: highly magnesian lithosphere-contaminated alkaline magmas from deep subcontinental mantle. Lithos 34:41–59

Arndt NT, Kerr AC, Tarney J (1997) Dynamic melting in plume heads: the formation of Gorgona komatiites and basalts. Earth Planet Sci Lett 146:289–301

Arndt N, Chauvel C, Czamanske G, Fedorenko V (1998) Two mantle source, two plumbing systems: tholeiitic and alkaline magmatism of the Maymecha River basin, Siberian flood volcanic province. Contrib Mineral Petrol 133:297–313

Barton JM Jr, Klemd R, Allsopp HL, Auret SH, Copperthwaite YE (1987) The geology and geochronology of the Annandagstoppane granite, Western Dronning Maud Land, Antarctica. Contrib Mineral Petrol 97:488–496

Beattie P (1993) Olivine-melt and orthopyroxene-melt equilibria. Contrib Mineral Petrol 115:103–111

Boyd FR (1959) Hydrothermal investigations of amphiboles. In: Abelson PH (ed) Researches in Geochemistry. John Wiley & Sons, New York, pp 377–396

Burke K, Dewey JF (1973) Plume-generated triple junctions: key indicators in applying plate tectonics to old rocks. J Geol 81:406–433

Carlson RW, Czamanske G, Fedorenko V, Ilupin I (2006) A comparison of Siberian meimechites and kimberlites: implications for the source of high-Mg alkalic magmas and flood basalts. Geochem Geophys Geosys 7. Doi:10.1029/2006GC001342

Coltice N, Phillips BR, Bertrand H, Ricard Y, Rey P (2007) Global warming of the mantle at the origin of flood basalts over supercontinents. Geology 35:391–394

Corner B (1994) Geological evolution of western Dronning Maud Land within a Gondwana framework: Geophysics subprogramme. Final project report to SACAR, Department of Geophysics, Witwaterstrand University, South Africa, p 21

Cox KG (1978) Flood basalts, subduction, and the break-up of Gondwanaland. Nature 274:47–49

Cox KG (1992) Karoo igneous activity, and the early stages of the break-up of Gondwanaland. In: Storey BC, Alabaster T, Pankhurst RJ (eds) Magmatism and the Causes of Continental Break-up. Geol Soc Spec Publ 68:137–148

Curtis ML, Riley TR, Owens WH, Leat PT, Duncan RA (2008) The form, distribution and anisotropy of magnetic susceptibility of Jurassic dykes in H.U. Sverdrupfjella, Dronning Maud Land, Antarctica. Implications for dyke swarm emplacement. J Struct Geol 30:1429–1447

Duncan RA, Hooper PR, Rehacek J, Marsh JS, Duncan AR (1997) The timing and duration of the Karoo igneous event, southern Gondwana. J Geophys Res B 102:18, 127–18, 138

Eggins SM (1992) Petrogenesis of Hawaiian tholeiites: 2, aspects of dynamic melt segregation. Contrib Mineral Petrol 110:398–410

Elkins-Tanton LT (2005) Continental magmatism caused by lithospheric delamination. In: Foulger GR, Natland JH, Presnall DC, Anderson DL (eds) Plates, Plumes and Paradigms. Geol Soc of Am Spec Paper 388, pp 449–462.

Elkins-Tanton LT, Draper DS, Agee CB, Jewell J, Thorpe A, Hess PC (2007) The last lavas erupted during the main phase of the Siberian flood volcanic province: results from experimental petrology. Contrib Mineral Petrol 153:191–209

Falloon TJ, Danyushevsky LV (2000) Melting of refractory mantle at 1.5, 2 and 2.5 GPa under anhydrous and H_2O-undersaturated conditions: implications for high-Ca boninites and the influence of subduction components on mantle melting. J Petrol 41:257–283

Falloon TJ, Danyushevsky LV, Ariskin A, Green DH, Ford CE (2007) The application of olivine geothermometry to infer crystallization temperatures of parental liquids: Implications for the temperature of MORB magmas. Chem Geol 241:207–233

Fedorenko V, Czamanske G (1997) Results of new field and geochemical studies of the volcanic and intrusive rocks of the Maimecha–Kotuy area, Siberian flood-basalt province (Russia). Int Geol Rev 39:479–531

Ford CE, Russell DG, Craven JA, Fisk MR (1983) Olivine-liquid equilibria: temperature, pressure and composition dependence of the crystal/liquid cation partition coefficients for Mg, Fe^{2+}, Ca and Mn. J Petrol 24:256–265

Foulger G (2007) The 'Plate' model for the genesis of melting anomalies. In: Foulger G, Jurdy D (eds) The Origins of Melting Anomalies: Plumes, Plates, and Planetary Processes. Geol Soc of Am Spec Paper 430, pp 1–28

Furnes H, Vad E, Austrheim H, Mitchell JG, Garmann LF (1987) Geochemistry of basalt lavas from Vestfjella and adjacent areas, Dronning Maud Land, Antarctica. Lithos 20:337–356

Gibson SA (2002) Major element heterogeneity in Archean to Recent mantle plume starting-heads. Earth Planet Sci Lett 195:59–74

Gibson SA, Thompson RN, Dickin AP (2000) Ferropicrites; geochemical evidence for Fe-rich streaks in upwelling mantle plumes. Earth Planet Sci Lett 174:355–374

Gilbert MC, Helz RT, Popp RK, Spear FS (1982) Experimental studies of amphibole stability. In: Veblen DR, Ribbe PH (eds) Amphiboles: Petrology and Experimental Phase Relations. Rev in Min 9B. Min Soc of Am, pp 229–354

Green DH, Falloon TJ, Eggins SM, Yaxley GM (2001) Primary magmas and mantle temperatures. Eur J Min 13:437–451

Groenewald PB, Moyes AB, Grantham GH, Krynauw JR (1995) East Antarctic crustal evolution: geological constraints and modelling in western Dronning Maud Land. Precamb Res 75:231–250

Gualda GAR, Vlach SRF (2005) Stoichiometry-based estimates of ferric iron in calcic, sodic-calcic and sodic amphiboles; a comparison of various methods. An Acad Bras Cienc 77:521–534

Hanski EJ (1992) Petrology of the Pechenga ferropicrites and cogenetic Ni-bearing gabbro-wehrlite intrusions, Kola Peninsula, Russia. Geol Soc of Finland Bull 367, p 192

Harris C, Marsh JS, Duncan AR, Erlank AJ (1990) The petrogenesis of the Kirwan Basalts of Dronning Maud Land, Antarctica. J Petrol 31:341–369

Heinonen JS, Luttinen AV (2008) Jurassic dikes of Vestfjella, western Dronning Maud Land, Antarctica: geochemical tracing of ferropicrite sources. Lithos 105:347–364

Herzberg C, Asimow PD (2008) Petrology of some oceanic island basalts: PRIMELT2.XLS software for primary magma calculation. Geochem Geophys Geosyst 9. Doi:10.1029/2008GC002057

Herzberg C, O'Hara MJ (1998) Phase equilibrium constraints on the origin of basalts, picrites, and komatiites. Earth Sci Rev 44:39–79

Herzberg C, O'Hara MJ (2002) Plume-associated ultramafic magmas of Phanerozoic age. J Petrol 43:1857–1883

Herzberg C, Zhang J (1996) Melting experiments on anhydrous peridotite KLB-1: composition of magmas in the upper mantle and transition zone. J Geophys Res B 101:8271–8295

Herzberg C, Asimow PD, Arndt N, Niu Y, Lesher CM, Fitton JG, Cheadle MJ, Saunders AD (2007) Temperatures in ambient mantle and plumes: constraints from basalts, picrites, and komatiites. Geochem Geophys Geosys 8. Doi:10.1029/2006GC001390

Hirose K, Kawamoto T (1995) Hydrous partial melting of lherzolite at 1 GPa: the effect of H_2O on the genesis of basaltic magmas. Earth Planet Sci Lett 133:463–473

Horan MF, Walker RJ, Fedorenko VA, Czamanske GK (1995) Osmium and neodymium isotopic constraints on the temporal and spatial evolution of Siberian flood basalt sources. Geochim Cosmochim Acta 59:5159–5168

Jacobs J, Fanning CM, Henjes-Kunst F, Olesch M, Paech H (1998) Continuation of the Mozambique Belt into East Antarctica: Grenville-age metamorphism and polyphase Pan-African high-grade events in central Dronning Maud Land. J Geol 106:385–406

Jacobs J, Bauer W, Fanning CM (2003a) Late Neoproterozoic/early Palaeozoic events in central Dronning Maud Land and significance for the southern extension of the East African Orogen into East Antarctica. Precamb Res 126:27−53

Jacobs J, Fanning CM, Bauer W (2003b) Timing of Grenville-age vs. Pan-African medium- to high grade metamorphism in western Dronning Maud Land (East Antarctica) and significance for correlations in Rodinia and Gondwana. Precamb Res 125:1−20

Jourdan F, Feraud G, Bertrand H, Kampunzu AB, Tshoso G, Watkeys MK, Le Gall B (2005) Karoo large igneous province: brevity, origin, and relation to mass extinction questioned by new $^{40}Ar/^{39}Ar$ age data. Geology 33:745−748

Jourdan F, Bertrand H, Schaerer U, Blichert-Toft J, Feraud G, Kampunzu AB (2007a) Major and trace element and Sr, Nd, Hf, and Pb isotope compositions of the Karoo large igneous province, Botswana-Zimbabwe: lithosphere vs mantle plume contribution. J Petrol 48:1043−1077

Jourdan F, Feraud G, Bertrand H, Watkeys MK (2007b) From flood basalts to the inception of oceanization: example from the $^{40}Ar/^{39}Ar$ high-resolution picture of the Karoo large igneous province. Geochem Geophys Geosys 8. Doi: 10.1029/2006GC001392

Juckes LM (1972) The geology of north-eastern Heimefrontfjella, Dronning Maud Land. British Antarctic Survey, Scientific Reports 65, p 44

Kamenetsky VS, Crawford AJ, Meffre S (2001) Factors controlling chemistry of magmatic spinel: an empirical study of associated olivine, Cr-spinel and melt inclusions from primitive rocks. J Petrol 42:655−671

Kogarko LN, Ryabchikov ID (2000) Geochemical evidence for meimechite magma generation in the subcontinental lithosphere of Polar Siberia. J Asian Earth Sci 18:195−203

Kogiso T, Hirschmann MM, Pertermann M (2004) High-pressure partial melting of mafic lithologies in the mantle. J Petrol 45:2407−2422

Krynauw JR, Watters BR, Hunter DR, Wilson AH (1991) A review of the field relations, petrology and geochemistry of the Borgmassivet intrusions in the Grunehogna Province, western Dronning Maud Land, Antarctica. In: Thomson MRA, Crame JA, Thomson JW (eds) Geological Evolution of Antarctica. International Symposium on Antarctic Earth Sciences 5, Cambridge University Press, United Kingdom, pp 33−39

Larsen LM, Pedersen AK (2000) Processes in high-Mg, high-T magmas: evidence from olivine, chromite and glass in Palaeogene picrites from West Greenland. J Petrol 41:1071−1098

Lawver LA, Gahagan LM, Coffin MF (1992) The development of paleoseaways around Antarctica. In: Kennett JP, Warnke DA (eds) Antarctic Paleoenvironment: a Perspective on Global Change, Part 1. Antarctic Research Series 58, Am Geophys Union, pp 7-30

Le Bas MJ (2000) IUGS reclassification of the high-Mg and picritic volcanic rocks. J Petrol 41:1467−1470

Leake BE (1971) On aluminous and edenitic hornblendes. Min Mag and J of the Min Soc 38:389−407

Lee CA, Luffi P, Plank T, Dalton H, Leeman WP (2009) Constraints on the depths and temperatures of basaltic magma generation on Earth and other terrestrial planets using new thermobarometers for mafic magmas. Earth Planet Sci Lett 279:20−33

Lenardic A, Moresi LN, Jellinek AM, Manga M (2005) Continental insulation, mantle cooling, and the surface area of oceans and continents. Earth Planet Sci Lett 234:317–333

Luttinen AV, Furnes H (2000) Flood basalts of Vestfjella: Jurassic magmatism across an Archaean-Proterozoic lithospheric boundary in Dronning Maud Land, Antarctica. J Petrol 41:1271–1305

Luttinen AV, Ramo OT, Huhma H (1998) Neodymium and strontium isotopic and trace element composition of a Mesozoic CFB suite from Dronning Maud Land, Antarctica: implications for lithosphere and asthenosphere contributions to Karoo magmatism. Geochim Cosmochim Acta 62:2701–2714

Luttinen AV, Zhang X, Foland KA (2002) 159 Ma Kjakebeinet lamproites (Dronning Maud Land, Antarctica) and their implications for Gondwana breakup processes. Geol Mag 139:525–539

Maurel C, Maurel P (1982) Étude expérimentale de l'équilibre Fe^{2+}-Fe^{3+} dans les spinelles chromiferes et les liquides silicatés basiques coexistants, à 1 atm. Comptes Rendus de l'Académie des Sciences (Série 2) 295:209–212

McDonough WF, Frey FA (1989) Rare earth elements in upper mantle rocks. In: Lipin BR, McKay GA (eds) Geochemistry and Mineralogy of Rare Earth Elements. Rev in Min 21, Min Soc of Am, pp 100–145

McKenzie D, Bickle MJ (1988) The volume and composition of melt generated by extension of the lithosphere. J Petrol 29:625–679

Morelli A, Danesi S (2004) Seismological imaging of the Antarctic continental lithosphere: a review. Global Planet Change 42:155–165

Morgan WJ (1971) Convection plumes in the lower mantle. Nature 230:42–43

Putirka KD (2005) Mantle potential temperatures at Hawaii, Iceland, and the mid-ocean ridge system, as inferred from olivine phenocrysts: evidence for thermally driven mantle plumes. Geochem Geophys Geosys 6. Doi:10.1029/2005GC000915

Putirka K (2008a) Excess temperatures at ocean islands: implications for mantle layering and convection. Geology 36:283–286

Putirka KD (2008b) Thermometers and barometers for volcanic systems. In: Putirka KD, Tepley FJ III (eds) Minerals, Inclusions and Volcanic Processes. Rev in Min and Geochem 69, Min Soc of Am, pp 61–120.

Putirka KD, Perfit M, Ryerson FJ, Jackson MG (2007) Ambient and excess mantle temperatures, olivine thermometry, and active vs. passive upwelling. Chem Geol 241:177–206

Révillon S, Arndt NT, Chauvel C, Hallot E (2000) Geochemical study of ultramafic volcanic and plutonic rocks from Gorgona Island, Colombia: the plumbing system of an oceanic plateau. J Petrol 41:1127–1153

Richards MA, Duncan RA, Courtillot VE (1989) Flood basalts and hot-spot tracks: plume heads and tails. Science 246:103–107

Riley TR, Leat PT, Curtis ML, Millar IL, Duncan RA, Fazel A (2005) Early-middle Jurassic dolerite dykes from western Dronning Maud Land (Antarctica): identifying mantle sources in the Karoo large igneous province. J Petrol 46:1489–1524

Ryabchikov ID, Solovova IP, Kogarko LN, Bray GP, Ntaflos T, Simkin SG (2002) Thermodynamic parameters of generation of meymechites and alkaline picrites in the Maymecha-Kotui province: evidence from melt inclusions. Geochem Int 40:1031–1041

Salters VJM, Stracke A (2004) Composition of the depleted mantle. Geochem Geophys Geosys 5, Doi:10.1029/2003GC000597

Schumacher JC (1997) Appendix 2: The estimation of ferric iron in electron microprobe analysis of amphiboles. In: Leake BE, Woolley AR, Arps CES et al: Nomenclature of Amphiboles: Report of the Subcommittee on Amphiboles of the International Mineralogical Association Commission on New Minerals and Mineral Names. Eur J of Min 9:623–651

Semet MP, Ernst WG (1981) Experimental stability relations of the hornblende magnesiohastingsite. Geol Soc of Am Bull 92:71–74

Simkin T, Smith JV (1970) Minor-element distribution in olivine. J Geol 78:304–325

Sisson TW, Grove TL (1993) Experimental investigations of the role of H_2O in calc-alkaline differentiation and subduction zone magmatism. Contrib Mineral Petrol 113:143–166

Sobolev AV, Kamenetskaya VS, Kononkova NN (1991) New data on petrology of Siberia meimechites. Geochem Int 8:1084–1095

Stone WE, Deloule E, Larson MS, Lesher CM (1997) Evidence for hydrous high-MgO melts in the Precambrian. Geology 25:143–146

Sun SS, McDonough WF (1989) Chemical and isotopic systematics of oceanic basalts: implications for mantle composition and processes. In: Saunders AD, Norry MJ (eds) Magmatism in the Ocean Basins. Geol Soc Spec Publ 42:313–345

Thompson RN, Gibson SA (2000) Transient high temperatures in mantle plume heads inferred from magnesian olivines in Phanerozoic picrites. Nature 407:502–506

Thompson RN, Gibson SA, Dickin AP, Smith PM (2001) Early Cretaceous basalt and picrite dykes of the southern Etendeka region, NW Namibia: windows into the role of the Tristan mantle plume in Paraná-Etendeka magmatism. J Petrol 42:2049–2081

White RS, McKenzie DP (1989). Magmatism at rift zones: the generation of volcanic continental margins and flood basalts. J Geophys Res 94:7685–7729.

Wolmarans LC, Kent KE (1982) Geological investigations in western Dronning Maud Land, Antarctica - a synthesis. S Afr J Antarc Res Suppl 2, p 93

Zhang X, Luttinen AV, Elliot DH, Larsson K, Foland KA (2003) Early stages of Gondwana breakup: the $^{40}Ar/^{39}Ar$ geochronology of Jurassic basaltic rocks from western Dronning Maud Land, Antarctica, and implications for the timing of magmatic and hydrothermal events. J Geophys Res B 108. Doi:10.1029/2001JB001070